Magnetic tweezers for intracellular applications

Basarab G. Hosu and Károly Jakab
Department of Physics, University of Missouri, Columbia, Missouri 65211

Péter Bánki and Ferenc I. Tóth
*Research Institute for Solid State Physics and Optics, Hungarian Academy of Sciences, H-1525, Budapest,
P. O. B. 49, Hungary*

Gabor Forgacs[a]
Department of Physics and Biology, University of Missouri, Columbia, Missouri 65211

We have designed and constructed a versatile magnetic tweezer primarily for intracellular investigations. The micromanipulator uses only two coils to simultaneously magnetize to saturation micron-size superparamagnetic particles and generate high magnitude constant field gradients over cellular dimensions. The apparatus resembles a miniaturized Faraday balance, an industrial device used to measure magnetic susceptibility. The device operates in both continuous and pulse modes. Due to its compact size, the tweezers can conveniently be mounted on the stage of an inverted microscope and used for intracellular manipulations. A built-in temperature control unit maintains the sample at physiological temperatures. The operation of the tweezers was tested by moving 1.28 μm diameter magnetic beads inside macrophages with forces near 500 pN. © *2003 American Institute of Physics.* [DOI: 10.1063/1.1599066]

I. INTRODUCTION

A magnetic tweezer is a device capable of exerting a force of controlled magnitude and direction on magnetic particles. Due to the simplicity of their operation, low cost of construction, and versatility, magnetic tweezers have recently gained popularity in probing biological materials at various scales. Most applications to date aim at the physical properties of (i) single molecules,[1–4] (ii) filamentous macromolecular networks,[5–9] or (iii) cell surfaces.[10–15] Intracellular properties have mostly been investigated indirectly, using test particles attached to the cytoskeleton through transmembrane receptors.[10,16,17] Very few tweezers have been built to reliably explore the intracellular environment directly.[18–20] There exist other powerful techniques, like optical tweezers and atomic force microscopes that can equally be used for applications [(i)–(iii)]. The advantages of magnetic micromanipulators become evident when intracellular properties are investigated. Optical tweezers exert force on microscopic objects that are transparent to (laser) light. Since there is a myriad of such objects inside a cell, optical tweezers cannot selectively operate in the intracellular environment. Atomic force microscopes, by their very nature, cannot be used to scan the interior of a cell.

In a typical intracellular application, magnetic beads are delivered inside living cells and moved (translated or rotated) with the tweezers. The trajectory of motion is recorded and subsequently analyzed in terms of well-established models of viscoelasticity.[12,18,21] This approach yields local information on the viscosity and elastic properties of the cytoplasm. The contribution of various intracellular components (e.g., cytoskeletal filaments, like actin or microtubules) can be assessed by controlled modifications of the interior of the cell (e.g., use of cytoskeleton depolymerizing agents, or by functionalizing the beads to bind to specific molecules).[10,17,19] By using beads of varying sizes, information can be gained on the local intracellular geometry. Systematic measurements of local viscoelastic parameters can be used to monitor possible abnormal transformations inside the cell.

The successful intracellular application of magnetic tweezers depends on the following factors. First, the magnetic particle has to be inserted into the cell without causing adverse effects. This is typically achieved by microinjection or by letting cells endocytose the particles. Second, prior to exposing the bead to the magnetic force of the tweezers, it has to be magnetized. This is typically accomplished by using separate magnetizing magnets and force or torque producing magnets. As a consequence, when magnetic coils are used to produce the desired magnetic fields, at least two pairs are used, which makes the apparatus bulky and difficult to manipulate.

Magnetic micromanipulators can either rotate or translate particles. In the first case, the magnetic moment of the particle is aligned in a particular direction and then exposed to a perpendicular constant magnetic field. This causes the bead to rotate. Viscoelastic properties of the environment of the bead are evaluated from the analysis of this circular motion. To displace a magnetic particle is more complicated. For this, a spatially varying magnetic field is needed albeit with the extra benefit of being able to study larger regions with a single bead. Viscoelastic properties are determined from the recorded trajectory of the particle.

Motivated by the large number of potential applications,

[a]Electronic mail: forgacsg@missouri.edu

we have constructed a translational magnetic tweezer with its primary use for intracellular manipulations. Our objective was to produce a device which is simultaneously simple, inexpensive, and powerful.

II. OPERATION OF THE TWEEZERS

A. Theoretical considerations

The force acting on a paramagnetic particle in a spatially varying magnetic field is

$$\mathbf{F}_M = \nabla(\mathbf{m}\cdot\mathbf{B}) = \nabla(mB). \tag{1}$$

The second equality is the consequence of the induced moment $m = MV$ being parallel to the magnetic induction vector B. Here M and V are, respectively, the magnetization and volume of the particle. If in the region of interest B is large enough so that M reaches its saturation value, furthermore $B_y = 0$ and $B_z = $ constant, then Eq. (1) reduces to

$$F_y = VM_x \frac{\partial B_x}{\partial y}. \tag{2}$$

It is Eq. (2) that forms the basis of the operation of our tweezers.

B. Design

We designed our tweezers with the following requirements in mind:

(1) To provide a high constant magnetic gradient over typical cellular dimensions (10–500 μm) capable of generating forces strong enough to displace beads trapped inside cells;
(2) To provide a strong enough magnetic field capable of magnetizing superparamagnetic beads to saturation;
(3) To be able to adjust and finely tune both the intensity of the magnetic field and the magnetic gradient during measurements to adapt to varying local conditions without interfering with data collection;
(4) To be able to generate both continuous magnetic fields and magnetic pulses;
(5) To have a sufficiently compact size to fit onto the stage of an inverted microscope without interfering with the functionality of the microscope or video acquisition hardware; and
(6) To be able to control the sample temperature.

Requirements 1 and 2 assure that the force acting on the magnetic particle during its motion is constant [see Eq. (2)], making the calibration of force in each measurement needless and data analysis simple.

Our magnetic tweezers workstation is shown in Fig. 1. The apparatus itself consists of a measuring unit and a control unit. The measuring unit is mounted on the stage of an Olympus IX-70 inverted microscope and connected to the control unit. Data is acquired through a digital video camera attached to the microscope and fed into a computer.
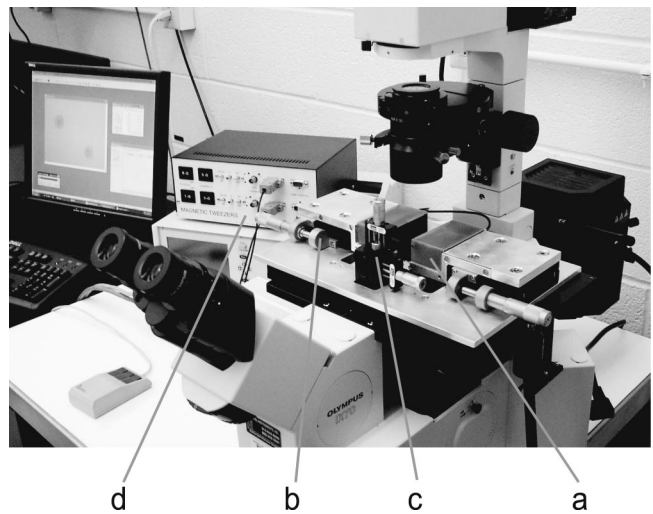

FIG. 1. Magnetic tweezers work station. The measuring unit is composed of two coils (a) [the separation between which can be fine tuned with micrometers (b)] and a sample holder (c). (d) Control unit.

C. Measuring unit

The measuring unit is shown schematically in more detail in Fig. 2. It contains two magnetic coils housed in fiberglass boxes and the sample holder [Figs. 1(a) and 1(b), respectively]. Glue is poured into the plastic boxes to prevent the displacement of the coils. The sample is located between the two pole pieces (see Fig. 2), which are continuations of
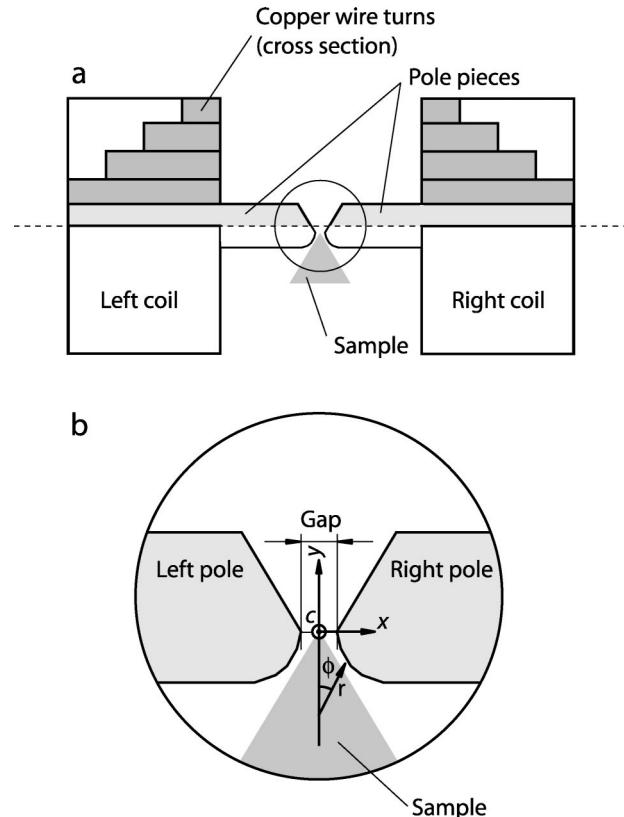

FIG. 2. Schematic representation of the measuring unit: (a) top view. The special coil structure is symmetric with respect to the broken line; details below the broken line are not shown. (b) Details of the pole piece profile; C—central point. The shaded triangle in (a) and (b) represents the shape and location of the sample holder.
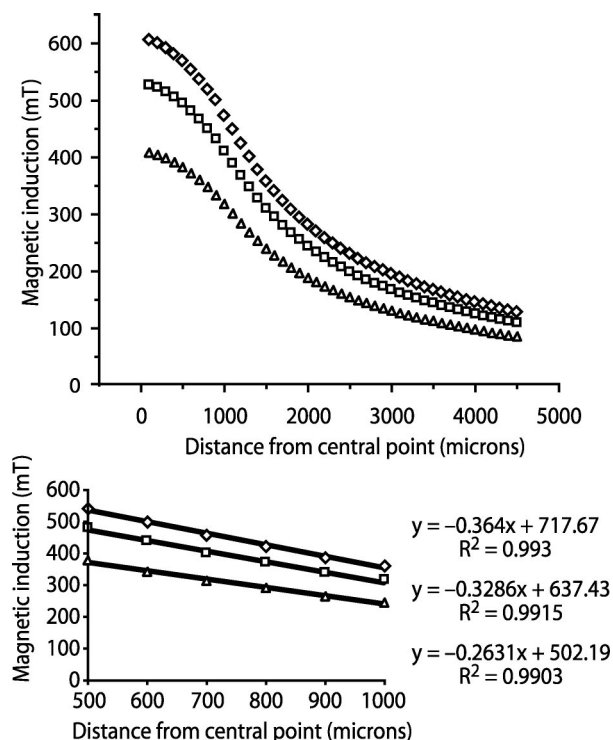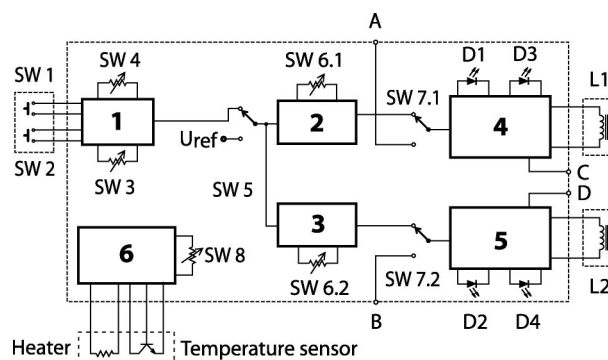
FIG. 4. Block diagram of the control unit. 1—Pulse generator; 2, 3—preamplifiers; 4, 5—voltage/current converters and power amplifiers; 6—temperature control unit; L1, L2—coils; SW1—pulse train trigger; SW2—manual pulse trigger; SW3—pulse length adjustment; SW4—time between pulses adjustment; SW5—pulse/continuous magnetic field switch; SW6.1 and SW6.2—current adjustment; SW7.1 and SW7.2—external/internal pulse switch; SW8—temperature adjustment; A, B—external pulse inputs; C, D—current monitor outputs; U_{ref}—internal dc reference for continuous field. Indicators (light): $D1$, $D2$–pulse monitor LED; $D3$, $D4$—overload LED.

FIG. 3. Magnetic induction at 500 μm gap distance for different currents through the coils: Triangles—1 A, squares—2 A, diamonds—3 A. The lower panel shows the region where the magnetic gradient is constant.

the metallic cores of the coil outside the boxes. The length of the pole pieces (21 mm each) is chosen to assure that a standard objective in an inverted microscope can be brought all the way to the sample even when the poles touch. This eliminates the need to use high working distance objectives. The position of the sample holder relative to the pole pieces is adjusted by a micromanipulator. The stage of the sample holder embeds a temperature sensor and a heating resistor connected to the control unit. The gap between the pole pieces can be varied by two additional micromanipulators, each controlling the position of one of the black boxes (see Fig. 1). The coils are made of copper wire (diameter $= 0.85$ mm) and have 720 turns; their resistance (R) and induction (L) are, respectively, 2.59 Ω and 7.2 mH. The special shape of the coil structure (see Fig. 2) provides an enhanced magnitude axial field and minimal coil time constant ($\tau = L/R$). The latter fact assures the possible quick rise of the magnetic field to its maximum value upon the switching on of the current through the coils. The cross sections of the metallic core and pole piece are respectively 8×8 mm^2 and 8×1.2 mm^2. They are made of 0.3 mm thick sheets of oriented (3% Si) silicon–iron alloy; a standard transformer core material with coercive field strength of 100 mA/cm and permeability 2000 at 50 Hz (Vacuumschmelze GmbH-Hanau, Germany). Sheets are glued together to minimize power loss. This material is chosen for its high saturation induction of 2.05 T.

The special profile of the pole pieces shown in Fig. 2 assures a constant magnetic gradient over extended regions and $B_y = 0$ along the midline (y direction) as well as a negligible variation of B_z on z between the poles (see Figs. 3

and 6). The constant magnetic gradient is larger in the lower (curved) region, which is machined according to the equation $r^{3/2} \sin(3\phi/2) = $ constant (for notations, see Fig. 2).[22] (All of the results given next refer to the curved region.) In essence, our tweezer is a miniaturized horizontally positioned Faraday balance, an industrial device used to measure the susceptibility of magnetic powders.[23]

D. Control unit

The control unit supplies the two coils with currents ranging from 0.1 to 4.1 A. Its core component is the pulse generator, unit 1 in Fig. 4. A pulse train is triggered by the switch (SW) SW1, a momentary push-button switch. Single pulses can be generated manually by the repeated activation of SW2. The pulse length and the interval between pulses can be adjusted with dials SW3 and SW4, respectively. The pulse length can be varied between 0.1 and 9.9 s in steps of 0.1 s. Switches SW1 and SW2 can conveniently be activated by means of a regular three-button computer mouse connected to the control unit. The simultaneous activation of the third button, with one of the "switch" buttons, generates sound during the pulse. The signal of the pulse generator is applied to preamplifiers (units 2 and 3 for the two coils respectively in Fig. 4), which control its amplitude in the range 0–4.1 V, regulated by means of dials SW6.1 and SW6.2 (one for each channel) in 0.1 V steps. The voltage pulses are eventually converted into current pulses through the coils by units 4 and 5 (voltage/current converters and power amplifiers). The conversion rate is 1 V for 1 A so that, after calibration, the dials SW6.1 and SW6.2 directly show the output current. The power amplifiers represent constant current sources and provide steady current through the coils during the entire pulse length. This is accomplished by an appropriate negative feedback loop. As the current is constant, both the magnetic field intensity and the magnetic gradient are constant during the pulse. Consequently, the magnetic force that acts on a magnetic bead is also constant during the magnetic

pulse. The control unit also contains a temperature regulating circuit (unit 6 in Fig. 4) that operates the temperature sensor and the heating resistor in the sample holder.

The described magnetic tweezer has a modular structure. Modules can be used separately and, if specific parameters for specific experiments are required, external modules can be used. For instance, inputs for external pulse generators are available if applications call for pulses shorter than 0.1 s or longer than 9.9 s. Output for monitoring the currents through the coils or synchronizing the pulses with the video acquisition pulses is also available. Each of the two coils is controlled separately. Pole pieces can be changed and different geometries can be tested. The apparatus can also use a single coil for applications in which having a constant magnetic gradient is not a requirement.

III. FORCE CALIBRATION

In order to perform meaningful quantitative measurements, the magnetic tweezer has to be calibrated: The force acting on a magnetic test particle has to be known at each instant of the measurement. As discussed in connection with Eq. (2), the magnetic force depends on both the magnetic gradient produced by the tweezers and the magnetic moment of the magnetic object. Our test particles are superparamagnetic (magnetite) beads of 1.28 μm diameter (Bangs Laboratories, Fishers, IN). There are three methods that we currently employ for force calibration.

A. Direct measurement

The straightforward way to determine the magnetic force is to independently measure the magnetization and the magnetic gradient of the bead. Since our tweezers, by design, provide a constant magnetic gradient along the y direction, we measured $B_x(y)$ using a high precision Gauss meter (FW Bell Model 7010, Bell Technologies, Orlando, FL). In this method, the lower limit on the distance between the poles is constrained to 500 μm by the thickness of our transverse Hall probe (model STF71-0204-05-T, Bell Technologies, Orlando, FL) that is inserted between them (see Fig. 3). The probe has a rectangular area of 2.0×2.7 mm^2; it hangs from a holder, which can be moved with micrometer precision along the midline between the poles. We match the center of this area (which provides the most accurate reading of the field strength) with the central point C (Fig. 2). The curves shown in Fig. 3 were obtained by displacing the probe along the y direction and acquiring data every 100 μm. (Data points separated by 10 μm give a curve with identical slope.) The measurements shown in Fig. 3 (performed at a 500 μm gap) indicate that the field intensity with high accuracy ($R^2 \approx 1$) is linear for at least 500 μm.

The magnetization of the magnetic beads was measured using a superconducting quantum interference device (SQUID). Results are shown in Fig. 5. A comparison of Figs. 3 and 5 indicates that, already at the 500 μm gap distance, the magnetic beads are saturated and thus, according to Eq. (2) the resulting magnetic force is constant over typical cell dimensions (10–500 μm).
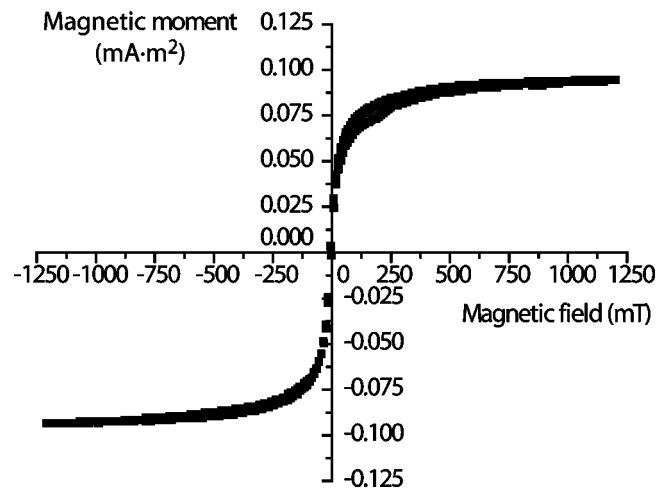

FIG. 5. Induced magnetization as measured by SQUID. The apparatus measured the total induced moment (y axis) of a 20 μl suspension of 1.28 μm beads with concentration 5.509×10^{-10} bead/mL. From this the average saturation magnetic moment of a single bead is $m = 7.26 \times 10^{-14}$ A m^2 and the saturation magnetization of the bead's material is $M = 6.6 \times 10^4$ A m.

B. Calibration using Stokes' law

The force produced by the tweezers increases rapidly with the decrease of the gap distance (see Fig. 6). To investigate this dependence and calibrate the tweezers for pole gaps smaller than 500 μm, we used Stokes' law. The magnetic force F_M, acting on a magnetic bead moving in a fluid, is counterbalanced by the viscous force given by the Stokes formula, thus

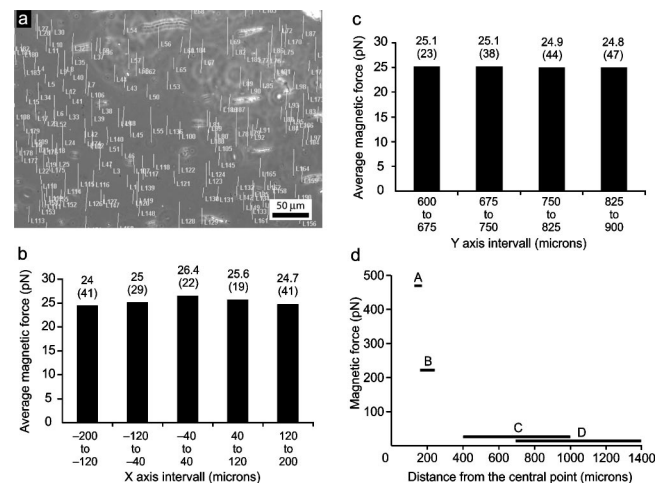$$F_M = MV\frac{\partial B_x(y)}{\partial y} = 6\pi\eta r v. \tag{3}$$

FIG. 6. Magnetic force measurement by using Stokes' law. (a) Bead trajectories in sucrose solution during a 1 s magnetic pulse (at 3 A current and 500 μm gap between the poles). The small spread in the length of the trajectories indicates the varying magnetic content of the beads. Microscopic images were acquired in bright field. Each vertical line represents a bead trajectory. [(b) and (c)]. Binned trajectories along the x (b) and y (c) direction. Numbers at the top of the bins indicate the average force and the number of particles (in brackets) for each bin. (d) Magnetic forces on 1.28 μm superparamagnetic beads for different gaps between poles: A=150 μm, B =200 μm, C=500 μm, and D=1000 μm. The horizontal lines show the extent of the constant gradient regions. Distance from the central point is measured along the y direction defined in Fig. 2.
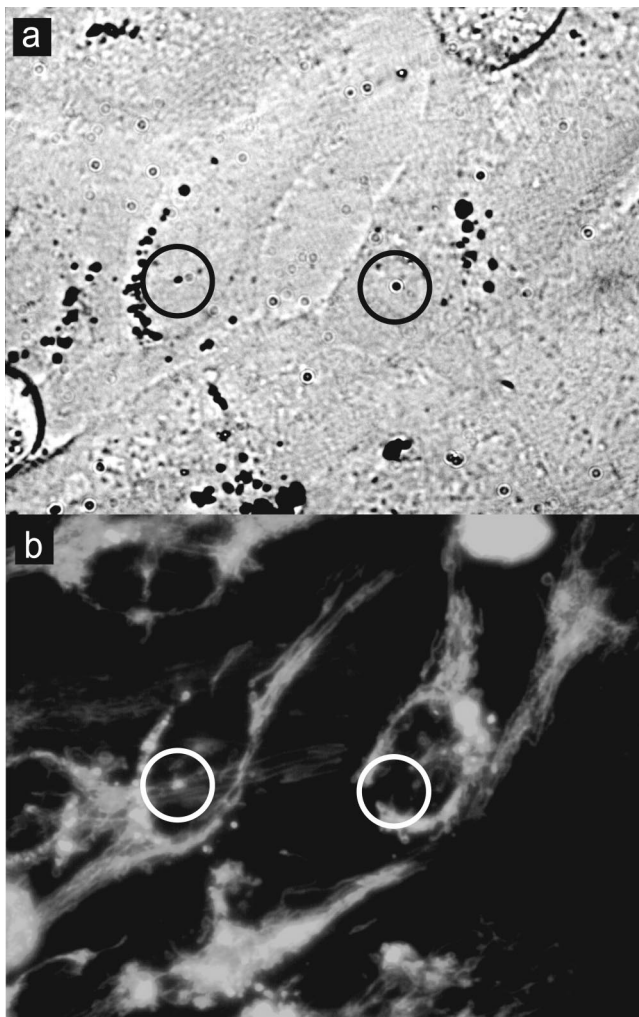
FIG. 7. Locating internalized beads. (a) Two magnetic particles carrying the FM 1-43 fluorescent endocytic marker are identified in bright-field microscopy (when they appear black and cellular details are barely visible) as potentially having been internalized by cells. (b) The same image in fluorescent mode. Only the particle on the left-hand side is visible, thus only that one has been internalized.
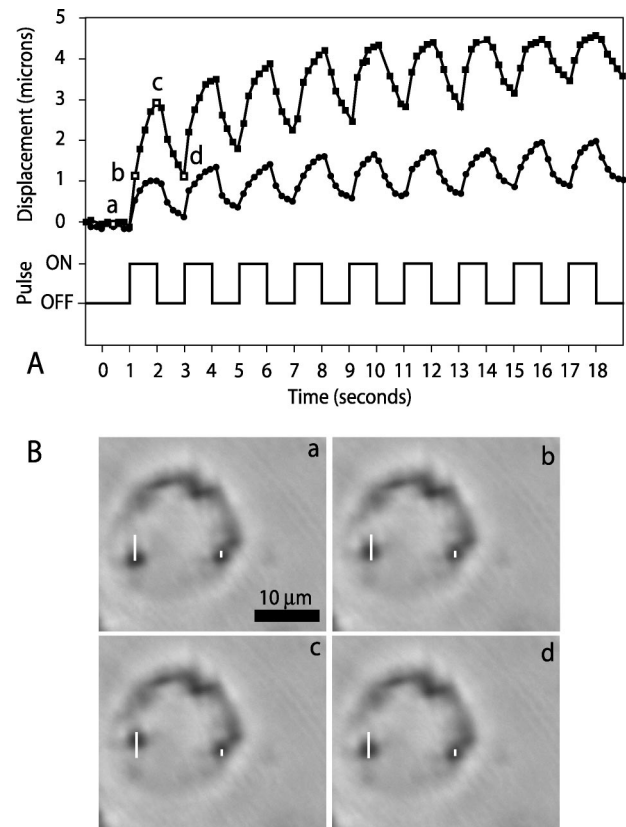

FIG. 8. Tweezers induced displacement of beads inside a macrophage. (A) Intracellular trajectory of two superparamagnetic beads (top traces) during 1 s magnetic pulses (bottom trace). Note the fast rise of the signal, which is due to the special configuration of the coils, shown in Fig. 2. (B) Sequence of images showing bead displacements. The two white vertical lines denote the total displacement of each bead. The instantaneous position of the bead on the left in (a), (b), (c), and (d) correspond to times marked by open squares in the upper trace in (A). The instantaneous location of the bead on the right at the same times is determined from the lower trace in (A). Images were acquired by bright-field microscopy using an Olympus LCPlanFL 60X objective (numerical aperture=0.7, working distance=1.1–1.89 mm). Bright-field microscopy provided no details on the intracellular environment, thus facilitating bead tracing. The 3 A 1 Hz current pulses with a 200 μm gap distance produced 220 pN force on 1.28 μm beads. The cells were located 250 μm from the central point C [which is within the region where the magnetic gradient is constant, see Fig. 6(d)] along the midline between the poles (see Fig. 2).

Here η, r, and ν are, respectively, the viscosity of the fluid, the radius of the bead, and its velocity. Stokes' formula is correct in the absence of interactions between beads (i.e., small bead concentration) and when the particle moves far from the walls of the container. Under conditions used for calibration there was no need for corrections to Stokes' formula.

Beads were introduced into chambers made of two triangular cover slips attached to each other by double-sided adhesive tape, resulting in container height of 100 μm. The sample holder and the chambers were designed to assure no contact between the pole pieces and tissue culture medium containing cells and thus avoid undesirable displacements due to magnetostriction manifest upon turning on the current. The velocities of a large number of beads were measured in different magnetic fields, by following the trajectory of their motion using videomicroscopy.

The shape of the chamber allowed us to finely decrease the gap distance to very small values (by the use of the attached micrometers shown in Fig. 1). As shown in Fig.

6(d), the location of the constant magnetic gradient region with respect to the central point and its extent depend on the gap distance. (Extrapolation to smaller gap distances indicates that a force in excess of 1 nN can be exerted on 1.28 μm beads, which is constant over typical cellular dimensions of 20–30 μm.) For the calibration, we used sucrose solutions, whose viscosities are known as function of concentration in the range 1–148 cP.[24] We employed Eq. (3) for gap distances larger than 500 μm as a consistency check. Once the Stokes force and the field gradient (as measured directly with the Hall probe) are known, Eq. (3) yields M. Performing the measurements in the magnetic field region where, according to Fig. 5, the magnetization should reach its saturation value, Eq. (3) gave results consistent with the SQUID data.

Figure 6(a) shows 152 trajectories in a rectangular area of 400×300 μm^2, centered along the y axis 750 μm down-

ward from the central point C in Fig. 2, in a region of linear magnetic field intensity as determined by the direct measurements (Fig. 3). To establish criteria for the linearity of the magnetic field when using Stokes' law for calibration, these trajectories were binned in both the horizontal and vertical direction. Figure 6(b) shows the 80 μm wide bins in the x direction, up to 200 μm to the left- and right-hand side of the midline between the poles. Figure 6(c) shows the same procedure along the y direction, where the width of the bins is 75 μm. As the results indicate, the spatial variation in the magnitude of the force are less than 10% along the x direction and around 1% along the y direction in the region shown in Fig. 6(a). A similar procedure and criteria were used to establish the full extension of the constant gradient region along the y axis, as shown in Fig. 6(d).

The magnetic force can also be determined by solving the Maxwell equations in the region between the poles. This calculation, complicated by the nontrivial shape of the poles, is presently under way and uses the method of finite elements.

IV. TESTING

Beads were spread over and incubated with cultured cells (under standard tissue culture conditions) in petri dishes and their location relative to the cells was checked after 48 h. Bead and cell concentrations were adjusted to have four beads/cell. We tested our tweezers by following the motion of 1.28 μm spherical superparamagnetic particles phagocytosed[18,19,25] by mouse macrophages [purchased from the American Tissue Culture Collection (ATCC), Manassas VI]. To make sure the beads indeed have been internalized by the cells and do not simply remain on the cell surface, we employed the fact that an object phagocytosed by a cell is packaged into an endocytic vesicle. Thus, we treated the macrophages with the fluorescent marker for endocytosis, FM 1-43 (Molecular Probes, Eugene, OR). This dye allows the direct visualization of endocytic vesicles,[26] as those surrounding the internalized beads. A bead is then first identified in the microscope under bright-field conditions. If, in fluorescence mode, it is still visible, then it has been internalized. This method is illustrated in Fig. 7.

Beads that were established to be inside cells were subjected to magnetic pulses of varying duration. Figure 8 shows the displacement of a bead inside a macrophage during the repeated application of 1 s magnetic pulses. The strongly viscoelastic nature of the cytoplasm is clearly manifested by the fact that the bead does not relax to its original location upon the turning off the field. Figure 8 illustrates the inhomogeneous nature of the interior of the cell. Beads at distinct locations, within the same cell, respond differently to the magnetic force. The local viscoelastic properties of the cytoplasm can be determined from the curves in Fig. 8 by standard methods.[12,19]

[1] S. B. Smith, L. Finzi, and C. Bustamante, Science **258**, 1122 (1992).
[2] T. R. Strick *et al.*, Biophys. J. **74**, 2016 (1998).
[3] C. Gosse and V. Coguette, Biophys. J. **82**, 3314 (2002).
[4] C. Haber and D. Wirtz, Rev. Sci. Instrum. **71**, 4561 (2000).
[5] F. Ziemann, J. Radler, and E. Sackmann, Biophys. J. **66**, 2210 (1994).
[6] F. G. Schmidt, F. Ziemann, and E. Sackmann, Eur. Biophys. J. **24**, 348 (1996).
[7] F. Amblard *et al.*, Rev. Sci. Instrum. **67**, 818 (1996).
[8] F. Amblard *et al.*, Phys. Rev. Lett. **77**, 4470 (1997).
[9] F. G. Schmidt, B. Hinner, and E. Sackmann, Phys. Rev. E **61**, 5646 (2000).
[10] N. Wang, J. P. Butler, and D. E. Ingber, Science **260**, 1124 (1993).
[11] M. A. Dichtl and E. Sackmann, Proc. Natl. Acad. Sci. U.S.A. **99**, 6533 (2002).
[12] A. R. Bausch *et al.*, Biophys. J. **75**, 2038 (1998).
[13] H. Huang *et al.*, Hypertension **38**, 1158 (2001).
[14] A. R. Bausch *et al.*, Biophys. J. **80**, 2649 (2001).
[15] V. M. Laurent *et al.*, Biomech. Eng. **124**, 408 (2002).
[16] A. J. Maniotis, C. S. Chen, and D. E. Ingber, Proc. Natl. Acad. Sci. U.S.A. **94**, 849 (1997).
[17] H. Huang *et al.*, Biophys. J. **82**, 2211 (2002).
[18] A. R. Bausch, W. Möller, and E. Sackmann, Biophys. J. **76**, 573 (1999).
[19] W. Möller *et al.*, Biophys. J. **79**, 720 (2000).
[20] O. A. Kuznetsov and K. H. Hasenstein, Adv. Space Res. **27**, 887 (2001).
[21] Y. C. Fung, *Biomechanics* (Springer, New York, 1993).
[22] D. E. Soule, C. W. Nezbeda, and A. W. Czanderna, Rev. Sci. Instrum. **35**, 1504 (1964).
[23] G. J. Hill, J. Sci. Instrum. **1**, 52 (1968).
[24] M. Mathlouthi and J. Génotelle, in *Sucrose Properties and Applications*, edited by M. Mathlouthi and P. Reiser (Blackie, London, 1995), pp. 126–154.
[25] W. C. Raschke, S. Baird, P. Ralph, and I. Nakoinz, Cell **15**, 261 (1978).
[26] T. Fergestad and K. Broadie, J. Neurosci. **21**, 1218 (2001).